Molecular modeling, synthesis, and activity studies of novel biaryl and fused-ring BACE1 inhibitors

Srinivas Reddy Chirapu [a,†], Boobalan Pachaiyappan [a,†], Hikmet F. Nural [b], Xin Cheng [b], Hongbin Yuan [a,†,‡], David C. Lankin [a], Samer O. Abdul-Hay [a], Gregory R. J. Thatcher [a], Yong Shen [b], Alan P. Kozikowski [a], Pavel A. Petukhov [a,*]

[a] *Department of Medicinal Chemistry and Pharmacognosy, College of Pharmacy, University of Illinois at Chicago, 833 S Wood Street, Chicago, IL 60612, USA*
[b] *Haldeman Laboratory of Molecular and Cellular Neurobiology, Sun Health Institute, Sun City, AZ 85351, USA*

ABSTRACT

A series of transition state analogues of beta-secretases 1 and 2 (BACE1, 2) inhibitors containing fused-ring or biaryl moieties were designed computationally to probe the S2 pocket, synthesized, and tested for BACE1 and BACE2 inhibitory activity. It has been shown that unlike the biaryl analogs, the fused-ring moiety is successfully accommodated in the BACE1 binding site resulting in the ligands with excellent inhibitory activity. Ligand **5b** reduced 65% of Aβ40 production in N2a cells stably transfected with Swedish human APP.

Memory loss is the most common characteristic in the clinical manifestation of Alzheimer's disease (AD) which affects the learning of both recent as well as recalled stored information.[1] It has been hypothesized that the therapeutic targeting of amyloid precursor protein (APP) processing may mitigate the formation of toxic fragments and prevents plaque formation. This large transmembrane protein can be cleaved at three distinct sites by proteolytic enzymes collectively referred to as 'secretases'.[2–5] The key enzyme crucial for the release of amyloidogenic fragments during APP processing is called β-secretase (BACE1).[2] BACE1 enzyme cleaves APP at the N-terminal side of the Aβ sequence to secrete sAPPβ, producing the cell-bound, carboxyl-terminal fragment C99 (also termed C100 or CTF).[3] The C99 fragment is then cleaved by the γ-secretase enzyme in the proteolytic cascade of APP processing. The resulting amyloid-beta peptides, called Aβ40 and Aβ42 because of the number of amino acids they are comprised of, form the extracellular neuritic amyloid plaques—one of the key factors in the pathogenesis of AD.[3]

It has been shown that BACE1 levels are significantly elevated in vivo in rapidly autopsied brains of sporadic AD patients (<3 h) compared with age-matched non-AD patients.[6–8] There has also been reports of a correlation ($R^2 = 0.54$) between BACE1 activity

and amyloid plaques count.[9] It was, therefore, suggested that lowering amyloid plaques in vivo may be achieved by a decrease in production of Aβ40 and Aβ42 through the inhibition of BACE1, thus opening up a new avenue for AD drug discovery.[10,11] The product of β-secretase cleavage, C99, also has toxic and pathogenic effects in transgenic mouse cells.[12,13] Another APP processing player, α-secretase, cleaves within the Aβ sequence to generate a large extracellular soluble fragment (sAPPα) and a smaller intracellular fragment (C83). These fragments appear to have no pathological significance, although sAPPα may have neuroprotective characteristics. A close-homolog of BACE1, BACE2, is thought to function as α-secretase by cleaving APP in the vicinity of the APP α-secretase cleavage site.[14,15] Due to its low concentration in the brain, it appears unlikely that BACE2 plays a significant role in the generation of Aβ40 or Aβ42,[16] however, it may play an important role in APP processing on the periphery affecting the muscle degeneration in AD patients.[17] Most of the known BACE1 inhibitors are relatively polar, non-selective and target other aspartic proteases including the highly homologous BACE2. Since BACE2 may serve as an alternative α-secretase, its inhibition is highly undesirable and needs to be addressed during the development of therapeutics that target BACE1. Multiple studies suggest that the physiologically relevant cleavage of APP by BACE1 occurs in endosomes where pH is optimal for BACE1 enzymatic machinery[18–22] or in cholesterol rich lipid rafts.[23] Therefore, further improvement of the cell membrane permeation properties of BACE1 inhibitors would be one of the most important tasks for lead optimization. A proof of principal

* Corresponding author. Tel.: +1 312 996 4174; fax: +1 312 916 7107.
E-mail address: pap4@uic.edu (P.A. Petukhov).
† All these authors contributed equally to this work.
‡ Present address: Burnham Institute, San Diego, CA, USA.

for an alternative to the passive permeation approach, a BACE1 inhibitor conjugated with a lipid fragment targeting endosomes, was recently reported by Simons and co-authors.[24]

The BACE1 binding site and a common binding pose of one of the recently developed BACE1 inhibitors is shown in Figure 1 (PDB code: 2B8L).[25] The in vitro and cell-based potencies, as reported by Stachel et al., are 15 and 29 nM, respectively.[25] In the course of our preliminary modeling efforts, we identified the S2 site (Fig. 1) as a potential target for further improvement of BACE1 activity and selectivity vs. BACE2. First, the BACE1 S2 site is formed by highly polar residues Asn233, Arg235, and Ser325, and is solvent-exposed. Many of the known ligands target S2 with polar groups that impose strict geometric requirements for their optimal binding. Replacing these polar substituents with either non-polar ones or groups that require only one or two hydrogen bonds would lead to less polar ligands in general. Second, the BACE1 S2 site contains a highly flexible residue Arg235, which adopts various conformations depending on the nature of P2 substituents. The extreme displacements of the Arg235 side-chains are observed in the X-ray structures of 2B8L and 1W51 and are shown in Figure 2. This observation suggests that the S2 site may accommodate novel scaffolds that would not otherwise be considered in the structure-based drug design efforts for BACE1 because they would poorly fit into the binding site. Third, despite the very large homology between BACE1 and BACE2 proteins the conformational changes that are induced by the ligands would not be identical and, thus, an improvement in selectivity may be observed.

Collectively, these observations prompted us to hypothesize that by lowering the number of polar groups we might gain more freedom in the positioning of the ligand since in this case the ligand has to form fewer highly directional hydrogen bonds. The loss in hydrogen bonding potential would, thus, be compensated for by non-directional van der Waals (vdW) interactions. In addition, compounds with fewer polar atoms are expected to have a more favorable drug-like profile. We also hypothesized that the increased flexibility of the residues in the S2 pocket makes it a perfect candidate for exploring different chemical scaffolds for further improvement activity, selectivity, and drug-like profile. To validate our hypothesis, we designed two series of compounds using computer-aided drug design, synthesized them, tested their activities against BACE1 and BACE2, and analyzed the results using molecular modeling methods. The results of these studies are described in this paper.

First, we established a strategy shown in Figure 3 to identify novel scaffolds which would allow us to verify our initial hypotheses. A software package for automated de novo design available in Sybyl,[26] Real-time Automated Combinatorial Heuristic Enhancement of Lead compounds (RACHEL),[27] was used to generate the new scaffolds. We elected to maintain the X and Y substituents in ligand 1, while allowing changes in portions A, B, and C (Fig. 3). The bridging group C was designed to maintain the orientation of the polar groups (if any) in positions A and B, to decrease the number of rotatable bonds, and to form an additional interaction with the binding site. The A, B, C fragments were allowed to be either 'nothing' (in case of the fragment C only), H, or a group selected from an in-house database of small molecule fragments. The RATOMS (number of ring atoms) descriptor of the chemical component corresponding to A, B, and C was set to minimum 5 and maximum 10. This database was generated by RACHEL from a set of drugs and drug-like small molecules found on the Drug-Bank web-site.[28] The RACHEL scoring function was amended to promote selection of cyclic structures by setting the maximum number of rotatable bonds to 4 and increasing the weight of the function from 1 to 4. We selected Asn233 as a target site for growing substituents and the molecular weight was limited to 200. The newly generated ligands by RACHEL were re-docked to the binding site using FlexX docking software. Among all potential ligands generated by RACHEL bi-cycles and biaryls stood out as groups of ligands having the binding poses similar to those found in BACE1 X-rays, targeting the S2 site, and having fewer or no hydrogen bond donors or acceptors. Upon visual inspection and evaluation of synthetic accessibility two scaffolds were selected for further synthetic elaboration: saturated bicycles with fused 6 or 7 ring systems containing a heteroatom and biaryls with 5- and 6-membered terminal aryl (Fig. 3). It was further decided not to use the actual FlexX docking score because (1) docking scores are typically less reliable compared with the accuracy of the binding poses prediction, and (2) we expected that the binding site residues in S2 may change their conformation to accommodate the new substituents. To explore if these new chemotypes are indeed compatible with the binding site of BACE1 two diverse series of biaryl and 5,6,7-membered bicyclic ligands shown in Table 1 were advanced for further medicinal chemistry efforts and biological testing.

The biaryl and fused-ring ligands were prepared using a common intermediate 12 according to a published procedure.[30] The synthesis of biaryl ligands is shown in Scheme 1. Commercially available substituted bromoisophthalic acid 7 was converted into 9 by (1) hydrolysis of 7 with 1 N NaOH which afforded the monoacid 8 and (2) subsequent coupling of 8 with (R)-α-methylbenzylamine in the presence of EDCA and HOBt resulting in the formation of 9. Intermediates 10 required for final products 2c and 3c were prepared by a Sonogashira coupling of bromide 9 with the mono TMS derivative of acetylene and phenylacetylene, respectively. Suzuki coupling of 3-thiopheneboronic acid or 4-chlorophenylboronic acid with 9 resulted in intermediates 10 required for the final products 3a and 3b. Sultam intermediates 10 required for the final products 4a and 4b were prepared by coupling 10 with the corresponding ring sultams. The final compounds 2c, 3a–3d, 4a–4b were obtained by hydrolysis of 10 to form the acid intermediate 11 followed by subsequent coupling with the TFA salt of (2R, 3S)-N-1-2-hydroxy-4-phenylbutane-1,3-diamine.[31–33] Compounds 2a and 2b were prepared using hydroxy and methoxy derivatives of diethyl esters of isophthalic acid in four steps: hydrolysis of one of the ester group with 1 N NaOH, coupling with the left side fragment (R)-α-methylbenzylamine, hydrolysis of the remaining ester group using 1 N NaOH, and finally coupling with the TFA salt of (2R, 3S)-N-1-2-hydroxy-4-phenylbutane-1,3-diamine.
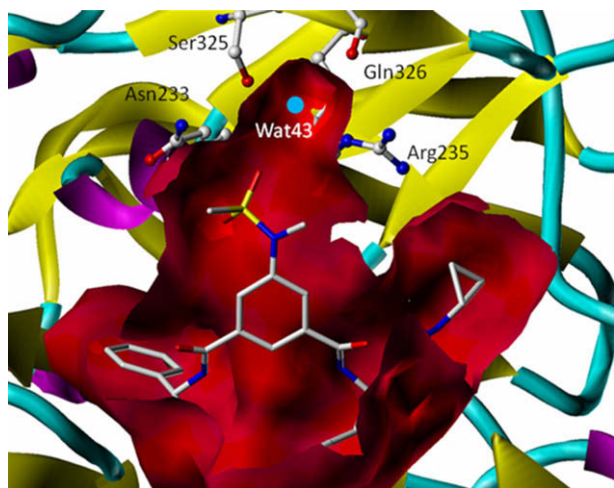
Figure 1. The binding site of BACE1, ligand 1, and a crystal water molecule in S2. The key residues in S2 site are rendered as 'ball and stick', whereas the ligand as 'capped sticks'. Water 43 is shown as blue sphere. The solvent accessible area of the binding site is rendered by red surface.
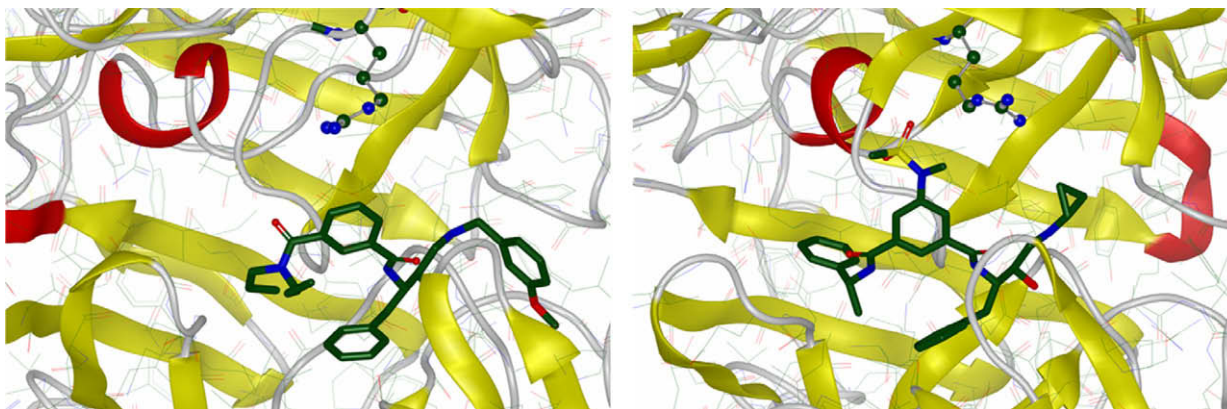
Figure 2. Two different conformations of Arg235 in BACE1 PDB structures 2B8L (left) and 1W51 (right) are rendered as capped sticks and are color coded (green, carbon; blue, nitrogen; red, oxygen; yellow, sulfur).
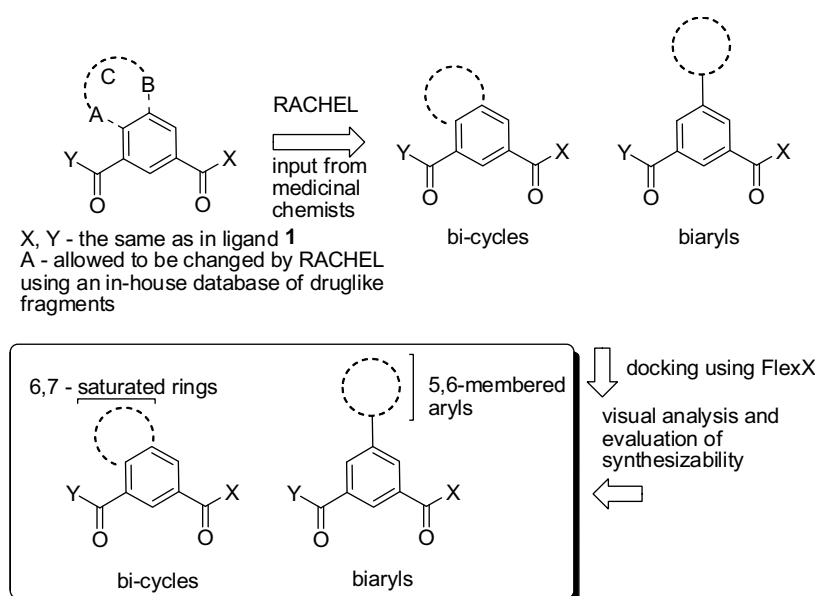
Figure 3. De novo design strategy utilized to find P2 fragments.

The bis-esters **15, 17**, and **19** were prepared according to the reported procedures starting from **14** (Scheme 2).[34,35] Subsequent selective hydrolysis of **17** yielded monoester **18a** as a major product whereas **19** resulted in monoester **20a** as a major product. Further treatment of **16a, 18a**, and **20b** with (R)-α-methylbenzylamine led to the corresponding intermediates **21–23** that upon hydrolysis and subsequent reaction with **12** resulted in the final products **5a, 5b**, and **6c** (Scheme 3). Reaction of **16b, 18b**, and **20a** with **12** resulted in intermediates **24–26** which upon hydrolysis and subsequent coupling with (R)-α-methylbenzylamine led to the final ligands **5c, 6a**, and **6b** (Scheme 4). The chemical characterization of compounds **5b**[36] and **5c**[37] is attached as a footnote.

Theoretically, two regioisomeric monoesters could have been produced from each diester **15, 17**, and **19** by hydrolysis of the right side ester or the left side ester. The structure of the hydrolysis products produced from **17** (Fig. 4b and c) and **19** were deduced in a self-consistent manner from the interpreted results of extensive NMR studies (1D ^{1}H and ^{13}C, 2D gCOSY, gHSQC, and gHMBC). The assignment strategy employed for the determination of the regioisomeric structure of the monohydrolysis products represents a straight forward approach involving: (1) unambiguous assignment the ^{1}H and ^{13}C NMR spectra for each of the hydrolysis products and

(2) the careful examination of the patterns of the $^3J_{C,H}$ correlations present in the gHMBC 2D spectrum of each of the hydrolysis products, specifically the correlations pertaining to the respective carbonyl carbons. In the generalized structure (n = 1 or 2; Fig. 4a), the aromatic ring proton located between both carboxylate carbons will exhibit $^3J_{C,H}$ correlations in the gHMBC to both carbonyl carbon signals (red and blue). The remaining aromatic ring proton (right side) will show the indicated $^3J_{C,H}$ correlation only to the carbonyl carbon on the right side (in red). If a carbonyl exists as an ester moiety, that is, with a methoxy group bonded to the carbonyl carbon, there will be an additional correlation cross peak in the gHMBC 2D spectrum arising from a $^3J_{C,H}$ coupling to the protons of the methoxy group to that carbonyl carbon. In this way, unambiguous assignment of the structure of the hydrolysis products can be made with confidence. This concept is illustrated for the starting dimethyl ester **17** (n = 1, R = R′ = Me), for which all of the ^{1}H and ^{13}C resonances were assigned.

In the case of the hydrolysis product **18a** derived from **17**, the 1D proton NMR spectrum (400 MHz, DMSO-d_6) confirmed the presence of three chemically distinct methylene groups with resonances centered at δ 1.921 (m), 3.027 (triplet, J = 5.2), and 4.175 (triplet, J = 6.6), each integrating for two (2) protons and all associ-

Table 1
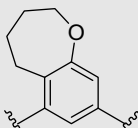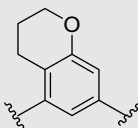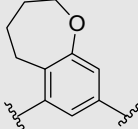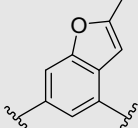BACE1 and BACE2 inhibition profile of P2 substituents.
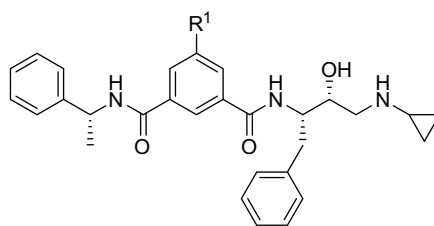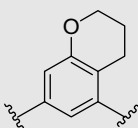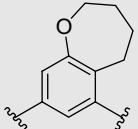
Ligands	R^1	BACE1 IC_{50} (nM)	BACE2 IC_{50} (nM)	log BB[a]
1		281 ± 42	132 ± 17	−0.9
2a	OH	1581 ± 269	>100,000	−0.8
2b	OMe	2506 ± 576	>100,000	−0.5
2c		889 ± 108	>100,000	−0.3
3a		2233 ± 384	>100,000	−0.6
3b		811 ± 102	>100,000	−0.1
3c		1119 ± 173	>100,000	−0.1
3d		1256 ± 140	>100,000	−0.5
4a		1774 ± 218	141 ± 16	−0.9
4b		158 ± 19	251 ± 33	−0.8

Ligands	-R^1-	R^2	BACE1 IC_{50} (nM)	BACE2 IC_{50} (nM)	log BB[a]
5a		H	524 ± 150	>100,000	−0.3
5b		H	63 ± 8	>100,000	−0.3

Table 1 (continued)

Ligands	-R^1-	R^2	BACE1 IC$_{50}$ (nM)	BACE2 IC$_{50}$ (nM)	log BB[a]
5c		H	56 ± 7	>100,000	−0.3
5d		F	740 ± 95	2089 ± 311	−0.3
5e		F	262 ± 36	1949 ± 207	−0.2
6a		H	998 ± 78	>100,000	−0.3
6b		H	112 ± 12	>100,000	−0.4
6c		H	89 ± 13	>100,000	−0.2

[a] Calculated log BB.

ated with the 6-membered ring present in the monohydrolyzed product. The gCOSY spectrum confirmed that the methylene groups constituted an isolated mutually coupled proton system. A singlet (3H) appearing at δ 3.837 was assigned to the methyl group of the monoester moiety. Two doublets were observed centered at δ 7.979 and δ 7.428 (J = 1.5 Hz), which were shown to be spin coupled (gCOSY) and were assigned to the two aromatic protons present on the aromatic ring. The magnitude of the J-coupling between the two aromatic protons confirmed the indicated *meta*-relationship. The protonated carbons could be assigned from the gHSQC spectrum ($^1J_{C,H}$) and gHMBC spectrum ($^2J_{C,H}$ and $^3J_{C,H}$). A broad resonance (1H) appeared at δ ~13 ppm and was assigned to the proton of the free acid. The gHMBC of hydrolysis product **18a** from **17** showed correlations from the proton at δ 7.979 to both of the carbonyl carbons at δ 166.2 and 166.3 ppm. There was a correlation observed from both the proton signal at δ 7.428 to the carbonyl carbon appearing at δ 166.3 as well as a correlation cross peak to the ester methyl group at δ 3.837 indicating that the hydrolysis of **17** proceeded at the left side carbonyl in the generalized structure. In contrast, the 1D proton NMR spectrum (400 MHz, DMSO-d_6) of the hydrolysis product **20a** from **19** confirmed the presence of four chemically distinct methylene groups with slightly broadened resonances centered at (δ 1.673, 1.899, 2.992–3.018 m, and 4.012 t (J = 6.6 Hz) each integrating for two (2) protons and all associated with the 7-membered ring present in the mono-hydrolyzed product from **19**. As in the case of **20a**, the

gCOSY spectrum confirmed that these resonances also constituted an isolated mutually coupled proton spin system. A singlet (3H) at δ 3.854 was assigned to the methyl group of the monoester moiety. Two signals were observed at δ 7.937 and δ 7.582, which were shown to be spin coupled (gCOSY) (J = 1.7 Hz) and which were assigned to the two aromatic protons present on the aromatic ring. The magnitude of the J-coupling between the two aromatic protons is also consistent with the indicated *meta*-relationship. Similar to the NMR of **18a**, the hydrolysis product of **17**, a broad resonance (1H) at δ ~13 ppm was also observed and was assigned to the proton of the expected free acid functionality. The protonated carbons could be easily assigned from the gHSQC spectrum ($^1J_{C,H}$). The gHMBC of hydrolysis product **20a** from **19** showed correlations from the proton at δ 7.937 to the both of the carbonyl carbons appearing at δ 166.0 and 167.2 ppm. There was a correlation observed from the proton signal at δ 7.582 to the carbonyl carbon at δ 166.0. The carbonyl at δ 167.2 also showed a correlation in the gHMBC spectrum to a methyl singlet (δ 3.854) indicating that the hydrolysis of **19** proceeded at the right side carbonyl (red, in the generalized structure). Analysis of the 2D gCOSY, gHSQC, and gHMBC data together with the 1D ^{1}H and ^{13}C NMR data obtained for both hydrolysis products permitted a self-consistent assignment of the ^{1}H chemical shifts and of the ^{13}C chemical shifts for both regioisomers. The ^{1}H and ^{13}C NMR assignments of intermediates **17** and **19** and their hydrolysis products **18a** and **20a** are shown in Figure 4d and e.
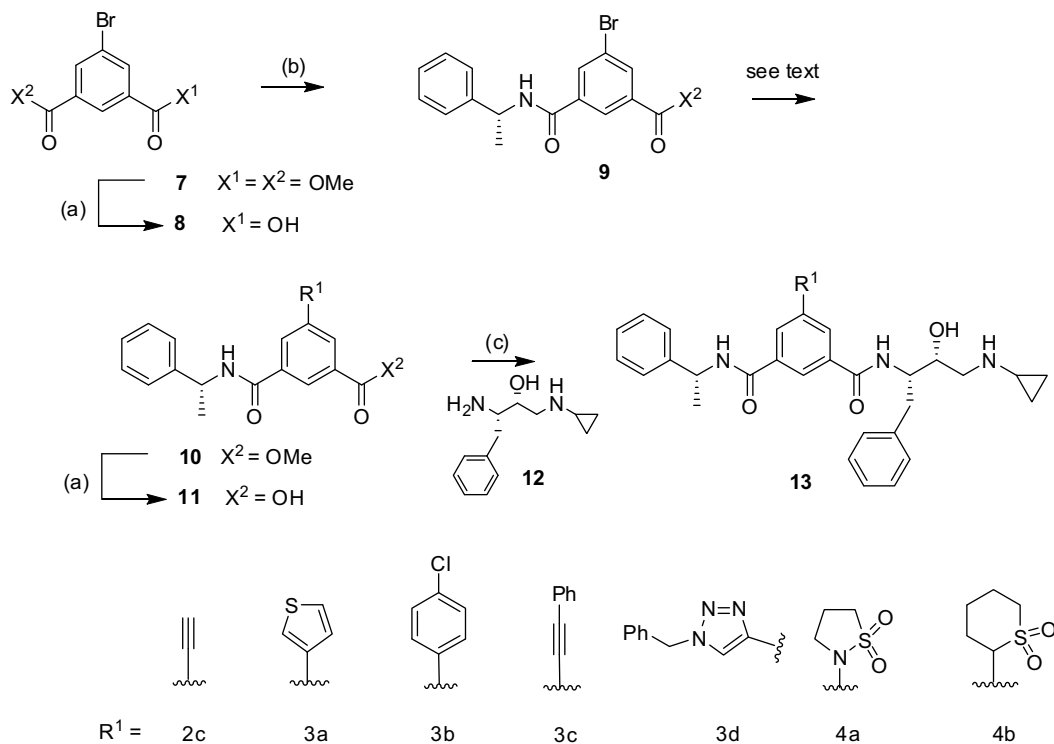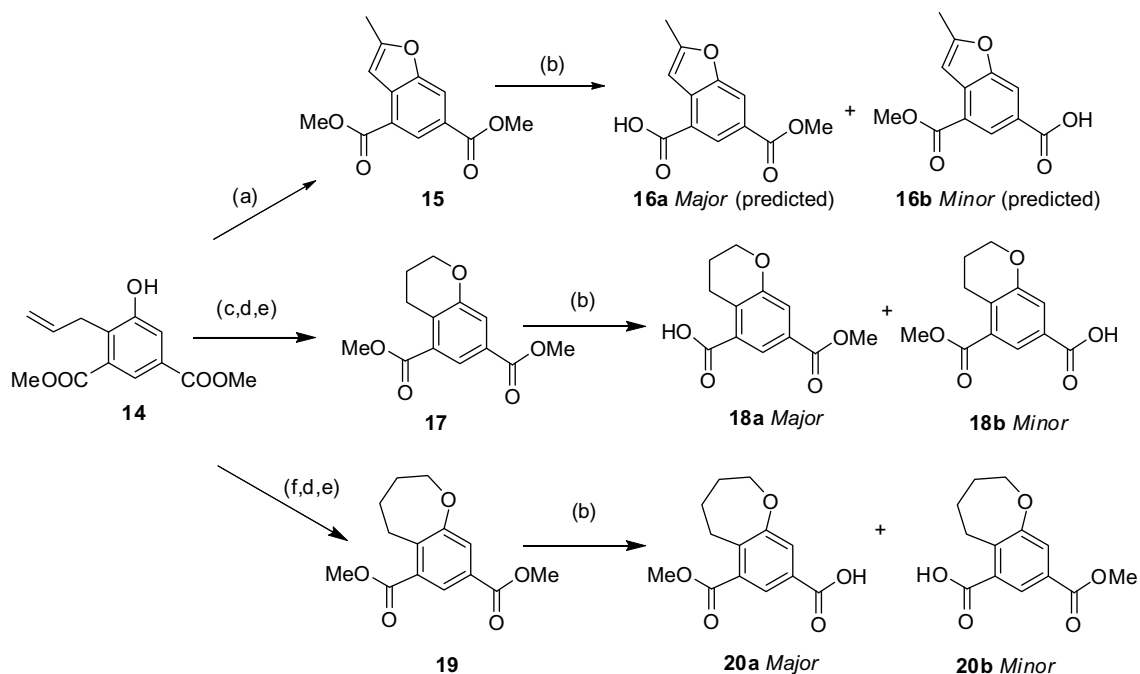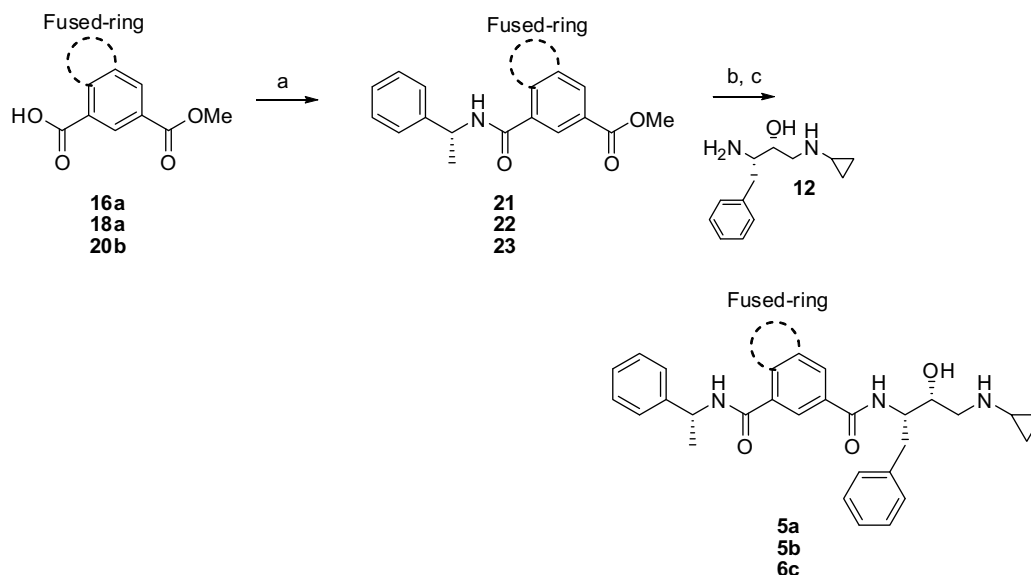
Scheme 1. Reagents and conditions: (a) 1 N NaOH; THF/MeOH (50:50) (90%); (b) (R)-α-methylbenzylamine, EDCA/HOBt, 0 °C to rt (92%); (c) **8**, EDCA/HOBt, 0 °C to rt (90%); (c) BOP, DIPEA (90%). In this and further schemes the typical yields of the reactions are provided in parentheses.

For IC$_{50}$ measurements, 293T cells stably transfected with pcDNA-BACE1 were maintained in 200 µg zeocin/ml DMEM, 10% FBS. Cells were lysed by lysis buffer (PBS with 1% Triton X100 and 0.1% SDS), and the lysate was adjusted to 4 µg/µl. The BACE1 inhibitors were diluted to the desired concentration with reaction buffer (100 mM Tris–HCl, 100 mM NaCl, pH 4.5). The consistent expression levels of BACE1 protein and enzyme activity were confirmed by BACE1 ELISA and BACE1 activity assay. We notice that pH 4.5 is not ideal for Tris buffer, however, we found that Tris buffer does not interfere with the activity and stability of the BACE1 (and BACE2) lysates at pH 4.5 necessary for their enzymatic activity.[2,9,38]

Scheme 2. Reagents and conditions: (a) PdCl$_2$, Cu(OAc)$_2$, LiCl, MeOH/H$_2$O (2 mL:0.1 mL) (85%); (b) 1 N NaOH; THF/MeOH (50:50), 0 °C to rt (80%); (c) tetravinyltin, Cu(OAc)$_2$, O$_2$, CH$_3$CN, 2 days (82%); (d) 2nd generation Grubbs catalyst, DCM, rt (80%)[29]; (e) H$_2$, Pd/C, MeOH (90%); (f) allyl bromide, K$_2$CO$_3$, acetone, reflux (96%).
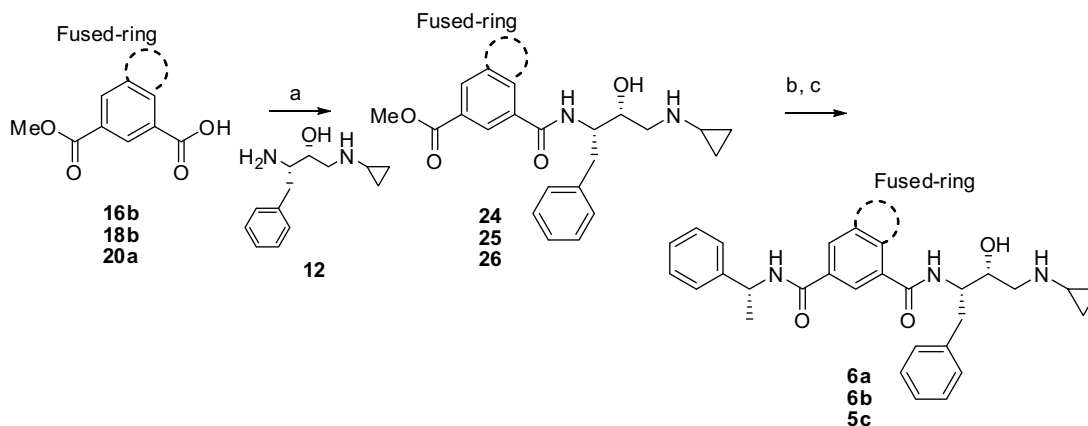
Scheme 3. Reagents and conditions: (a) (R)-α-methylbenzylamine, EDCA/HOBt, 0 °C to rt (92%); (b) 1 N NaOH; THF/MeOH (50:50), 0 °C to rt (90%); (c) EDCA/HOBt, 0 °C to rt (85%).

The BACE1 substrate (EDANS-SEVNLDAEFR-DABCYL) was dissolved in DMSO as stock and then diluted to 10 μM working solution. We then mixed 20 μg of 293T/pcDNA-BACE1 of cell lysate with BACE1 inhibitor and the substrate, and the final substrate concentration was 5 μM. Fluorescence was detected in microplate reader (Bio-tek) every 5 min at emission length 500 nm as well as excitation at about 430 nm. Again, the consistent expression levels of BACE1 protein and enzyme activity were confirmed by BACE1 ELISA and BACE1 activity assay. Maximal velocities were calculated by the time point within 20 min. Similarly, 293T cells stably transfected with pcDNA-BACE2 were maintained in 200 μg Geneticin (G148)/ml DMEM, 10% FBS. Cells were lysed by lysis buffer (PBS with 1% Triton X100 and 0.1% SDS), 5 μg protein were used in the assay. The BACE2 inhibitors were diluted to desired concentration with a reaction buffer (100 mM Tris–HCl, 100 mM NaCl, pH 4.5). The BACE2 substrate (MCA-ERHADGLALALEPA(K-Dnp) was dissolved in DMSO as stock. The cell lysate was mixed with BACE2 inhibitors and the substrate (final concentration 5 μM). Fluorescence was detected every 5 min at an emission length of 430 nm as well as excitation at about 340 nm. Maximal velocities were calculated by the time point within 20 min. The IC$_{50}$ of BACE1 and

BACE2 inhibition was then calculated and the results are shown in Table 1.

The following procedure was implemented to determine the efficacy of our best BACE1 inhibitors in reducing the Aβ40 production. Mouse neuroblastoma cells (N2a) stably transfected with Myc-epitope tagged Swedish mutant APP 695 cDNA (a kind gift from Dr. Gopal Thinakaran) were cultured in 1:1 Opti-MEM/Dulbecco's modified Eagle's medium (high glucose) containing 5% fetal bovine serum, 1% penicillin/streptomycin and 0.2 mg/ml G418 in a humified air incubator at 37 °C (5% CO$_2$–95% O$_2$). Cells were plated in 24 well plates for 24 h at a concentration of 15×10^4 cell/well. After 24 h, the growth medium was discarded and replaced with 0.5 ml of serum reduced medium consisting of Dulbecco's modified Eagle's medium (high glucose) and 0.2% fetal bovine serum. Fifteen minutes after medium replacement, the cells were treated with drugs dissolved in DMSO and incubated for 24 h. At the end of the incubation period, 100 μl of conditioned media were collected and the protease inhibitor AEBSF (4-(2-aminoethyl) benzene sulfonyl fluoride hydrochloride) was immediately added at a final concentration of 1 mM. The concentration of Aβ40 was determined using human beta amyloid [1–40] colorimetric ELISA kit from

Scheme 4. Reagents and conditions: (a) EDCA/HOBt, 0 °C to rt (90%); (b) 1 N NaOH; THF/MeOH (50:50), 0 °C to rt (95%); (c) (R)-α-methylbenzylamine, EDCA/HOBt, 0 °C to rt (90%).
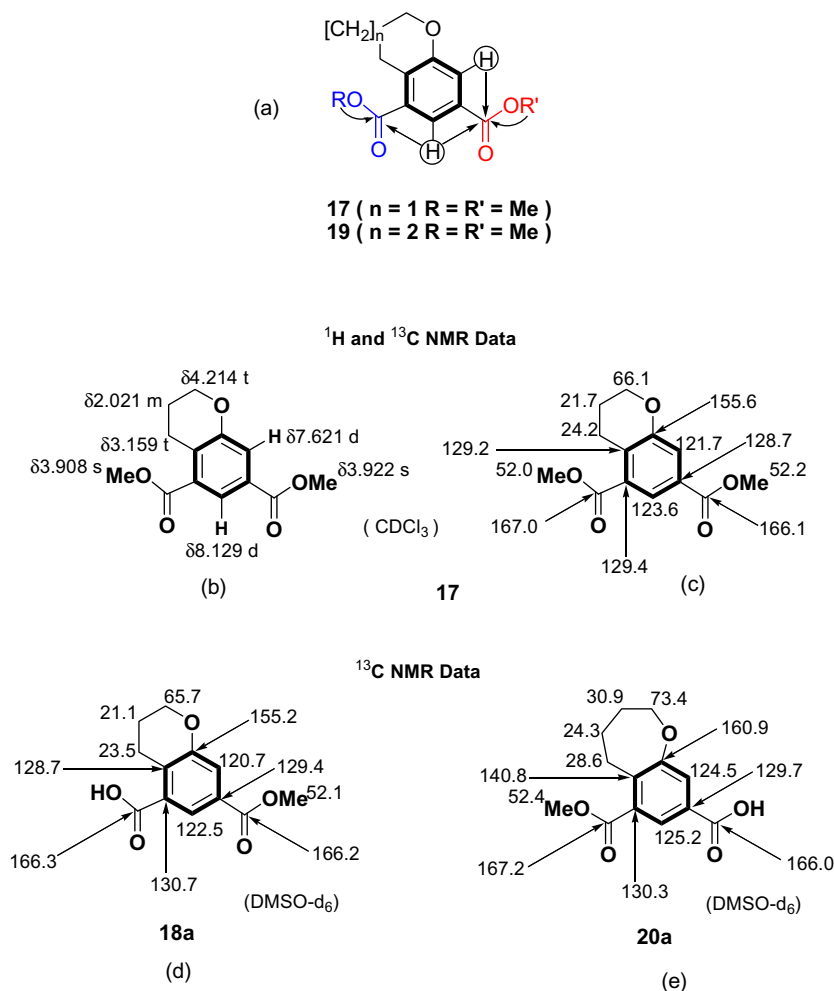
Figure 4. (a) General structure of ligands **17** and **19**; (b) ^{1}H NMR assignments for **17**; (c) ^{13}C NMR assignments for **17**; (d) ^{13}C NMR assignments for **18a**; (e) ^{13}C NMR assignments for **20a**.
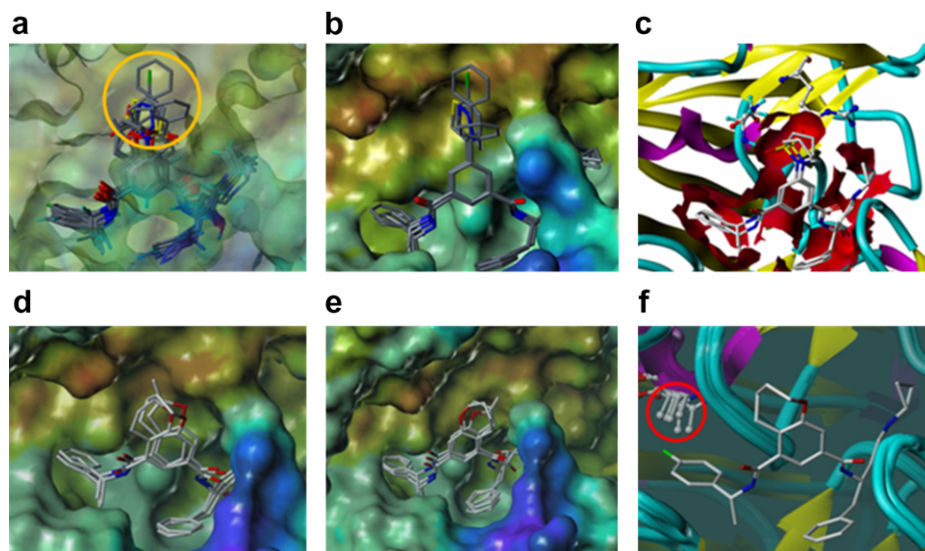
Figure 5. (a) Gold docked conformations of all ligands in BACE1 binding site. The P2 moieties are circled yellow; (b) biaryl compounds **3a–3d** in BACE1 binding site; (c) cyclic ring sultam compounds **4a–4b** in BACE1 binding site rendered as ribbon and tube representation. Residues Asn233 and Arg235 are rendered as ball-and-stick representations; (d) overlay of docked poses of ligands **5a–5c** when side-chain flexibility of Arg235 is considered; (e) overlay of docked poses of ligands **6a–6c** when side-chain flexibility of Arg235 is considered; (f) ligand **5e** in BACE1 binding site. Different orientations of methyl group in Ala335 observed in X-ray crystal structure is rendered as a ball-and-stick representation and circled in red for clarity.

Invitrogen. The procedure was followed as instructed in the supplied protocol.

The subsequent molecular modeling analysis was performed in the following way. The X-ray coordinates of BACE1 (PDB code: 2B8 L) were downloaded from the Protein Databank. The catalytic residue Asp32 was protonated according to the published theoretical studies.[39,40] The active site was defined as a sphere enclosing residues within 10 Å of the bound ligand. The 3D structures of ligands shown in Table 1 were built using Sybyl 7.3[26] and were energy minimized using BFGS algorithm, 5000 iterations, and gradient of 0.005 kcal/mol/Å as the termination criterion. The resulting minimized molecules were docked to the binding site of BACE1 using the GOLD software.[41] All poses outputted by the docking program were visualized; however, only the pose with the best fitness score was used for the following SAR analysis. Wherever appropriate, docking under induced-fit mode was applied to accommodate the side-chain flexibility of Arg235. Prior to the SAR analysis, the ability of the docking program to successfully reproduce the binding mode of the co-crystallized ligand **1** was evaluated. It was found that GOLD was able to reproduce the X-ray binding mode of co-crystallized **1** with a RMSD of 0.36 Å. We also calculated the log BB values to confirm that the new ligands exhibit improved blood–brain permeation properties. The log BB values of all inhibitors **1, 2a–2c, 3a–3d, 4a–4b, 5a–5e, 6a–6c** were calculated using Clark's equation.[42] The actual coefficients in the Clark equation were refitted using the original data in the Clark paper to account for the difference between the polar surface area and ClogP used by Clark and those generated by the Tripos software. The contact van der Waals surface area (cvdWSA) was calculated using MOLCAD separated surfaces between R^1 and the residues Thr231, Thr232, Asn233, Ser325, Arg235, Gln73, and Thr72 proximal to R^1. The figures were generated either with Vida 3.0 or with Sybyl8.0.

The best docking poses were visualized in the binding site (Figure 5a), and the SAR of the synthesized compounds is discussed below. Hydroxyethylamine (HE) motif is well known to mimic the transition state of the peptides cleaved by aspartic proteases, and it has been successfully employed in the BACE1 inhibitor design.[43] Multiple transition state analogs containing HE motif were crystallized. Our docking confirms that the binding modes of our ligands are similar to those found for the transition state analogs.

Substitution of R^1 by a simple hydroxyl or a methoxy group in **2a** and **2b** (Table 1) resulted in no activity at BACE2 and approximately 6- and 9-fold loss in BACE1 activity compared to ligand **1**, respectively, a relatively small trade-off in exchange of improvement of the drug-like profile and BACE1/BACE2 selectivity. The docking shows that the solvent-exposed hydroxyl or methyl group in **2a** and **2b** do not form favorable contacts with the binding site. In the induced-fit mode docking, the side-chain guanidine group of Arg235 is able to interact with the hydroxyl or methoxy groups in **2a** and **2b**, respectively. Substitution of R^1 in **1** with an acetylene moiety in **2c** led to a mere 3-fold decrease in BACE1 activity. As well as in the case of ligands **2a** and **2b** this is a small trade-off for replacing methyl sulfonamide group of **1** with a small acetylene group in **2c**. This observation supports our initial hypothesis that the loss of hydrogen-bonding contribution may be compensated by non-directional vdW interactions of the P2 substituents as a result of possible induced fit changes. Indeed, the docking shows that the P2 acetylene moiety forms extensive vdW contact with the alkyl side-chains of Arg235 and Thr231 located in S2. None of **2a–c** ligands showed BACE2 inhibition below 100 μM concentration. As expected, the relatively less polar **2a–c** are predicted to have better log BB of −0.3 compared to −0.9 for **1**.

Encouraged by these initial findings, we synthesized and tested ligands **3a–3d** to explore whether the S2 pocket can accommodate larger biaryl substituents. The docking poses of these compounds

are shown in Figure 5b. The 3-thiophene moiety in **3a** did not significantly influence the activity compared to **2b**. A replacement of R^1 with the bulkier *p*-chlorophenyl moiety in ligand **3b** led to a 3-fold increase in potency compared to **3a** and an almost equal activity to **2c**, a ligand with a smaller R^1 acetylene substituent. An analysis of the docking pose of **3b** shows that binding of its *p*-chlorophenyl substituent requires a displacement of the conserved water molecule WAT43 (in 2B8L) typically mediating hydrogen bonding between the side-chains of Ser325, Arg235, and Gln326 (discussed below). It is likely that an induced fit disorder caused by the removal of the conserved water molecule may contribute to improved binding energy of **3b**.[44] When the GOLD program was allowed to determine whether WAT43 should be bound or displaced upon binding of **3b**, the resulting ligand–protein complex did not contain WAT43. Probing of the binding site with larger, extended substituents as in the phenylacetylene- and *N*-benzyltriazole-containing ligands **3c** and **3d** resulted in a 1.4- and 1.6-fold loss of activity compared to **3b**, respectively. The loss was more pronounced in **3d** where the benzyl appendage appears to be completely solvent-exposed. Unlike **3c** and **3d**, ligands **3a** and **3b** fit well within the cleft of the S2 pocket. The predicted log BB values for the biaryl series range from modest −0.6 and −0.5 for compounds **3a** and **3d**, respectively, to −0.1 for both **3b** and **3c**. Similarly to ligands **2a–c** ligands **3a–d** are not active against BACE2 at concentrations up to 100 μM.

To explore the impact of rigidification/cyclization of the sulfonamide group of ligand **1** on BACE1 and BACE2, compare the resulting ligands with biaryls without sulfonamide group, and to find a future pharmacophore for the hot spot Asn233 (Leu246 in BACE2), we have tested two ring sultams **4a** and **4b**. The 6-membered sultam **4b** is found to be about 11-fold more active than 5-membered sultam **4**, 1.8-fold more active than ligand **1** at BACE1, and 1.9-fold less active at BACE2 than ligand **1**. The 5-membered sultam **4a**, on the other hand, was 12.6-fold more active at BACE2 than at BACE1. Sultam **4a** is exclusively BACE2 selective among all the ligands that were tested. Although it is not sufficient to talk about a general trend, it appears that a sulfonamide group has to be present in S2 to maintain the activity of the ligands at BACE2. An analysis of the binding modes of ligands shows that the SO_2 group in sultams points toward the S2 site whereas the alicyclic ring is solvent-exposed (Fig. 5c). This predicted mode of binding is very similar to the one that is observed in the X-ray crystal structure of the 6-membered sultam published during the preparation of this manuscript (PDB code: 2VNM). In **4b**, one of the SO_2 oxygen atoms forms a hydrogen-bond with backbone NH of Asn233 (N–O distance = 3.3 Å, N...H...O angle = 170°), whereas the other oxygen atom forms ion–dipole interactions with epsilon nitrogen (NE) of Arg235 (distance = 2.8 Å). Ligand **4a**, owing to its constrained 5-membered ring, forms a weak hydrogen bond with Asn233 (N–O distance = 3.7 Å, N...H...O angle = 142°) and weak ion–dipole interactions with NE of Arg235 (distance = 3.7 Å) and hence less active compared to **4b**. Further, the cvdWSA in $Å^2$ of **4a** and **4b** are 278 and 292, respectively. The calculated log BB values of compounds **4a** and **4b** are similar to that of ligand **1**.

Next, we synthesized a series of fused-ring compounds which were subsequently tested for the inhibition of BACE1 and BACE2 (Table 1). We synthesized and tested three sets of regioisomers that differ by the size and position of the ring fused to the central phenyl moiety. We found that the degree of lipophilicity and flexibility incorporated at the P2 position in **5a–5c** and their regioisomers **6a–6c** correlates with the BACE1 inhibitory activity of the ligands: (less lipophilic, less active) **5a** < **5b** < **5c** (more lipophilic, more active) and similarly **6a** < **6b** < **6c**. Upon docking using GOLD under induced-fit mode, it was found that ligands **5c** and **6c**, containing the more flexible 7-membered ring, form better vdW contact with the enzyme as compared with the ligands **5b** and **6b**,

which contain only a moderately flexible 6-membered ring. Ligands **5b** and **6b** possess more efficient vdW interactions with the binding site than their 5-membered ring analogs **5a** and **6a** (Fig. 5d and e). The cvdWSA in Å^2 calculated under the induced-fit mode for **5a–5c** are 183, 258, 266, whereas for compounds **6a–6c** it is 209, 197, and 227, respectively. The cvdWSA correlates with activity of compounds **5a–5c** but not **6a–6c** suggesting that this parameter alone is not sufficient to explain the trend in activity.

To find a plausible explanation for the difference in activity profiles of **5a–5c** and their regioisomers **6a–6c**, we analyzed the X-ray co-crystal structures of BACE1 protein available in Protein Data Bank. Two interesting observations resulted from this analysis. First, the group at the P2 position appears to control the position of Arg235 through an induced-fit effect. Depending on the steric bulk and electronic properties of the P2 substituent, Arg235 is forced to adopt different conformations. The maximum change in the location of Arg235 was observed between 1W51 and 2B8L with a deviation of 4.4 Å between the two guanidine carbon atoms in the Arg235 side-chain. Second, in those cases where the P2 has *N*-methylsulfonamide moiety (PDB codes: 1TQF, 2IRZ, 2B8L, 2IS0, 2NTR, 2OAH, 2P4J, 2P8H, and 2PH6), a conserved water molecule mediates hydrogen bond between the side-chains of Arg235, Ser325, and Gln326. On the other hand, if Arg235 changes its position as in 1W51 the water molecule is not observed in the crystal structures. It appears that both observations are interconnected—those ligands responsible for the movement of Arg235 also contribute to the displacement of the water molecule and loss of the hydrogen bonds between this water molecule and residues Ser325, Arg235, and Gln326. To account for the induced-fit effect Arg235 was allowed to change conformation during docking with Gold. Fused-ring compounds **5a–5c** has an oxygen atom locked in a position amenable for hydrogen bonding with side-chain NH$_2$ of Arg235. Our docking experiments suggest that in order to facilitate this hydrogen bond, Arg235 must lose its contact with water (WAT43 in 2B8L). Similar hydrogen-bonding interaction is not possible in regioisomers **6a–6c** because the ring precludes their contact with Arg235 and hence a near 2-fold drop in potency compared to **5a–5c** is observed. The calculated logBB is −0.3 for ligands **5a–5c** and −0.3, −0.4 and −0.2 for **6a–6c**, respectively. This shows improvement when compared to the ligand with the sulfonamide moiety bound to S2 pocket. As with the other ligands in the biaryl and fused-ring series that according to the docking experiments require an induced fit, ligands **5a–c** and **6a–c** did not show inhibition of BACE2.

Several publications have reported that fluorinated BACE1 inhibitors exhibited better activity than the non-fluorinated inhibitors due to increased lipophilicity.[30,45] Unlike the compounds described in these publications, both fluorinated compounds **5d** and

5e are found to be less active than non-fluorinated analogs **5b** and **5c** by ca. 5- and 12-fold, respectively. Ligand **5e** exhibits 2.8-fold better activity than **5d** perhaps for the same reasons **5c** is more active than **5a** and **5b**—larger area of contact with the binding site due to flexibility of the 7-membered ring. To understand what could be the reason for overall lower activity of **5d** and **5e** compared to their non-fluorinated analogs we visually inspected the crystal structures of BACE1 with different P2 substituents and found that the induced-fit effect of P2 affects the orientation of the methyl group in Ala335 (Fig. 5f). Of particular interest, the RMSD between CB atoms for crystal structures 2P8H (P3 = *p*-fluoro-α-methylbenzylamino, P2 = *N*-methylsulfonamide) and 2IQG (P3 = *N*,*N*-dipropanoyl and P2 = Me) is 1.2 Å. Because of the proximity of the methyl group in Ala335 and the fluorine atom in the BACE1 inhibitors, any conformational changes in S2 may result in mutual steric clashing. If an induced fit caused by the fused rings in series **5** and **6** takes place it may, indeed, affect the position of Ala 335 and explain the overall lower activity of the fluorinated compounds **5d** and **5e** compared to their non-fluorinated analogs. The predicted logBB values of **5d** and **5e** are almost the same as those of the non-fluorinated compounds. Unlike non-fluorinated fused-ring ligands in series **5** and **6**, both fluorinated ligands **5d** and **5e** showed a reasonable, ca. 2 μM, activity against BACE2.

To find a possible explanation for BACE1 selectivity of the ligands we tried to compare qualitatively the flexibility of the BACE1 and BACE2 proteins using their b-factors. A quantitative comparison of the b-factors is not possible since there is large number of the same residues in different X-ray structures of BACE1 proteins that differ in their b-factors depending on the co-crystallized ligand. It is clear, however, that the flexibility patterns for the residues in the S2 pocket and adjacent to it areas of the BACE1 and BACE2 proteins are different, suggesting that induced fit may play a role in an improved selectivity toward BACE1.

To investigate the effect of BACE1 inhibitors on APP processing the most active ligands **5b** and **5c** were tested for reduction in Aβ40 production in mouse neuroblastoma cells (N2a) transfected with Swedish mutant APP695 (Fig. 6). Compounds **5b** and **5c** reduce ca. 65% and 35% of Aβ production, respectively, compared to the control. At the moment it is unclear why almost equally active **5b** and **5c** exhibit 1.9-fold difference in reduction of Aβ40. It may be related to their metabolic stability or delivery to the site of action. This observation is being actively investigated at this time.

In summary, by using computer-aided drug design methods, we have designed, synthesized, tested the activity of the fused-ring and biaryl compounds against BACE1 and BACE2, and analyzed the resulting SAR using docking protocols. The fused-ring compounds are in general more active than the biaryl-based ligands with an activity range from 56 to 998 nM. This is comparable to the activity of the ligands with polar substituents occupying the S2 binding pocket, which lends support for our initial hypothesis that the S2 site may be targeted with less polar substituents. Most of the ligands displayed more favorable calculated logBB. The side-chain flexibility of Arg235 and, perhaps, adjacent residues, and possibly the presence of a water molecule mediating hydrogen bond interactions between Arg235, Ser325, and Gln326 in S2 appears to play an important role in accommodating the fused-ring and biaryl-based ligands in the binding site. Most of the fused-ring and biaryl-based ligands are BACE1 selective, and thus support our initial hypothesis that differences in the flexibility of BACE1 and BACE2 proteins and the ability to accommodate the ligands through induced fit can be utilized to design BACE1/2 selective ligands. In addition, it appears that the sulfonamide group is required to maintain BACE2 activity. The fused-ring ligands **5b** and **5c** combine the best attributes of acceptable logBB, BACE1 inhibitory activity, BACE2 selectivity, and ability to reduce the Aβ production. A similar approach may be used to explore other binding pockets of BACE1 (and BACE2) to
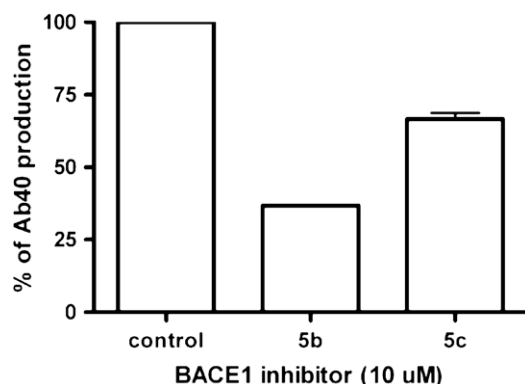
Figure 6. Reduction of Ab40 levels by BACE1 inhibitors detected in N2a cells stably transfected with Swedish human APP.

create new chemotypes for further development of therapeutics to treat AD and to serve as general probes for drug discovery.

Acknowledgments

References and notes

1. Petersen, R. C.; Smith, G. E.; Ivnik, R. J.; Kokmen, E.; Tangalos, E. G. *Neurology* **1994**, *44*, 867.
2. Vassar, R.; Bennett, B. D.; Babu-Khan, S.; Kahn, S.; Mendiaz, E. A.; Denis, P.; Teplow, D. B.; Ross, S.; Amarante, P.; Loeloff, R. *Science* **1999**, *286*, 735.
3. Selkoe, D. J. *Physiol. Rev.* **2001**, *81*, 741.
4. Vassar, R.; Citron, M. *Neuron* **2000**, *27*, 419.
5. Esler, W. P.; Wolfe, M. S. *Science* **2001**, *293*, 1449.
6. Li, R.; Lindholm, K.; Yang, L. B.; Yue, X.; Citron, M.; Yan, R.; Beach, T.; Sue, L.; Sabbagh, M.; Cai, H. *Proc. Natl. Acad. Sci. U.S.A.* **2004**, *101*, 3632.
7. Holsinger, R. M.; McLean, C. A.; Beyreuther, K.; Masters, C. L.; Evin, G. *Ann. Neurol.* **2002**, *51*, 783.
8. Fukumoto, H.; Cheung, B. S.; Hyman, B. T.; Irizarry, M. C. *Arch. Neurol.* **2002**, *59*, 1381.
9. Yang, L. B.; Lindholm, K.; Yan, R.; Citron, M.; Xia, W.; Yang, X. L.; Beach, T.; Sue, L.; Wong, P.; Price, D. *Nat. Med.* **2003**, *9*, 1.
10. Hardy, J.; Selkoe, D. J. *Science* **2002**, *297*, 353.
11. Vassar, R. *Adv. Drug. Deliv. Rev.* **2002**, *54*, 1589.
12. Suh, Y. H. *J. Neurochem.* **1997**, *68*, 1781.
13. Dewachter, I.; Reverse, D.; Caluwaerts, N.; Ris, L.; Kuiperi, C.; Van den Haute, C.; Spittaels, K.; Umans, L.; Serneels, L.; Thiry, E. *J. Neurosci.* **2002**, *22*, 3445.
14. Basi, G.; Frigon, N.; Barbour, R.; Doan, T.; Gordon, G.; McConlogue, L.; Sinha, S.; Zeller, M. J. *Biol. Chem.* **2003**, *278*, 31512.
15. Yan, R.; Munzner, J. B.; Shuck, M. E.; Bienkowski, M. J. *J. Biol. Chem.* **2001**, *276*, 34019.
16. Sun, X.; He, G.; Song, W. *FASEB J.* **2006**, *20*, 1369.
17. Vattemi, G.; Engel, W. K.; McFerrin, J.; Pastorino, L.; Buxbaum, J. D.; Askanas, V. *Exp. Neurol.* **2003**, *179*, 150.
18. Koo, E. H. *Traffic* **2002**, *3*, 763.
19. Small, S. A.; Gandy, S. *Neuron* **2006**, *52*, 15.
20. Kinoshita, A.; Fukumoto, H.; Shah, T.; Whelan, C. M.; Irizarry, M. C.; Hyman, B. T. *J. Cell. Sci.* **2003**, *116*, 3339.
21. Rajendran, L.; Honsho, M.; Zahn, T. R.; Keller, P.; Geiger, K. D.; Verkade, P.; Simons, K. *Proc. Natl. Acad. Sci. U.S.A.* **2006**, *103*, 11172.
22. He, X.; Cooley, K.; Chung, C. H.; Dashti, N.; Tang, J. *J. Neurosci.* **2007**, *27*, 4052.
23. Cheng, H.; Vetrivel, K. S.; Gong, P.; Meckler, X.; Parent, A.; Thinakaran, G. *Nat. Clin. Pract. Neurol.* **2007**, *3*, 374.
24. Rajendran, L.; Schneider, A.; Schlechtingen, G.; Weidlich, S.; Ries, J.; Braxmeier, T.; Schwille, P.; Schulz, J. B.; Schroeder, C.; Simons, M.; Jennings, G.; Knolker, H. J.; Simons, K. *Science* **2008**, *320*, 520.
25. Stachel, S. J.; Coburn, C. A.; Steele, T. G.; Crouthamel, M. C.; Pietrak, B. L.; Lai, M. T.; Holloway, M. K.; Munshi, S. K.; Graham, S. L.; Vacca, J. P. *Bioorg. Med. Chem. Lett.* **2006**, *16*, 641.
26. Sybyl7.3. Tripos Inc.: 1699 South Hanley Rd., St. Louis, Missouri, 63144, USA, 2006.
27. Chris M. W. Ho at Drug Design Methodologies, L. http://www.newdrugdesign.com/Technology.html, 2008.
28. Wishart, D.; Departments of Computing Science & Biological Sciences, University of Alberta, Canada, http://www.drugbank.ca/, 2007.
29. Groaz, E.; Banti, D.; North, M. *Adv. Synth. Catal.* **2007**, *349*, 142.
30. Stachel, S. J.; Coburn, C. A.; Steele, T. G.; Jones, K. G.; Loutzenhiser, E. F.; Gregro, A. R.; Rajapakse, H. A.; Lai, M. T.; Crouthamel, M. C.; Xu, M. *J. Med. Chem.* **2004**, *47*, 6447.
31. Miroshnikova, O. V.; Hudson, T. H.; Gerena, L.; Kyle, D. E.; Lin, A. J. *J. Med. Chem.* **2007**, *50*, 889.
32. Thorand, S.; Krause, N. *J. Org. Chem.* **1998**, *63*, 8551.
33. Steinhuebel, D.; Palucki, M.; Askin, D.; Dolling, U. *Tetrahedron Lett.* **2004**, *45*, 3305.
34. Blouin, M.; Frenette, R. *J. Org. Chem.* **2001**, *66*, 9043.
35. van Otterlo, W. A. L.; Ngidi, E. L.; Kuzvidza, S.; Morgans, G. L.; Moleele, S. S.; de Koning, C. B. *Tetrahedron* **2005**, *61*, 9996.
36. *Chroman-5,7-dicarboxylic acid 7-[(1-benzyl-3-cyclopropylamino-2-hydroxy-propyl)-amide]5-[(1-phenyl-ethyl)-amide (**5b**):* 1H NMR (300 MHz, MeOD): δ 7.12–7.40 (m, 12H), 5.23 (q, J = 7.1 Hz, 1H), 4.08–4.17 (m, 3H), 4.3 (m,1H), 4.08–4.17 (m, 2H), 3.77–3.75 (m, 1H), 3.25–3.31 (m, 2H), 2.96–2.77 (m, 4H), 2.26–2.14 (m, 2H), 1.59 (d, J = 7.0 Hz, 3H), 1.80–2.14 (m, 1H), 0.5–0.4 ppm (m, 4H). ^{13}C NMR(CDCl$_3$, 75 MHz): δ 6.4, 6.5, 21.8, 22.2, 22.8, 31.0, 36.4, 52.0, 49.1, 54.3, 66.6, 71.5, 116.9, 117,4, 124.3, 126.7, 126.9, 128.2, 128.3, 128.7, 128.9, 128.8, 129.0, 129.5, 129.7, 129.6, 133.24, 133.6, 139.5, 139.5, 155.4, 169.3 ppm; ESI-HRMS calculated for [C$_{32}$H$_{37}$N$_3$O$_4$ + H]$^+$: 528.2697, found: 528.2648. HPLC purity 97%.
37. *2,3,4,5-Tetrahydro-benzo[b]oxepine-6,8-dicarboxylic acid 6-[(1-benzyl-3-cyclopropylamino-2-hydroxy-propyl)-amide] 8-[(1-phenyl-ethyl)-amide] (**5c**):* 1H NMR (300 MHz, MeOD): δ 7.43–7.18 (m, 12H), 5.23 (q, J = 7.1 Hz, 1H), 4.3 (m, 1H), 4.01–3.92 (m, 2H), 3.76–3.74 (m, 1H), 3.25–2.69 (m, 4H), 2.46–2.44 (m, 2H), 2.25–2.24 (m, 1H), 1.90–2.14 (m, 2H),1.57 (d, J = 7.8 Hz, 3H), 0.50–0.40 (m, 4H). ^{13}C NMR (CDCl$_3$, 75 MHz): δ 4.24, 4.38, 22.0, 22.1, 25.3, 29.7, 30.2, 29.7, 31.6, 32.1, 35.6, 49.2, 52.3, 54.3, 69.3, 74.1, 115.6, 115.9, 121.1, 121.5, 127.2, 128.1, 128.2, 129.1, 129.5, 132.3, 137.5, 138.5, 138.6, 139.4, 161.2, 168.2, 168.8 ppm; ESI-HRMS calculated for [C$_{29}$H$_{34}$N$_4$O$_4$ + H]$^+$: 542.6874, found: 542.6866. HPLC purity 97%.
38. Yan, R.; Bienkowski, M. J.; Shuck, M. E.; Miao, H.; Tory, M. C.; Pauley, A. M.; Brashier, J. R.; Stratman, N. C.; Mathews, W. R.; Buhl, A. E.; Carter, D. B.; Tomasselli, A. G.; Parodi, L. A.; Heinrikson, R. L.; Gurney, M. E. *Nature* **1999**, *402*, 533.
39. Rajamani, R.; Reynolds, C. H. *J. Med. Chem.* **2004**, *47*, 5159.
40. Polgár, T.; Keserü, G. M. *J. Med. Chem.* **2005**, *48*, 3749.
41. Jones, G.; Willett, P.; Glen, R. C.; Leach, A. R.; Taylor, R. *J. Mol. Biol.* **1997**, *267*, 727.
42. Clark, D. E. *J. Pharm. Sci.* **1999**, *88*, 807.
43. Yang, W.; Lu, W.; Lu, Y.; Zhong, M.; Sun, J.; Thomas, A. E.; Wilkinson, J. M.; Fucini, R. V.; Lam, M.; Randal, M.; Shi, X. P.; Jacobs, J. W.; McDowell, R. S.; Gordon, E. M.; Ballinger, M. D. *J. Med. Chem.* **2006**, *49*, 839.
44. Crespo, A.; Fernandez, A. *Mol. Pharm.* **2008**, *5*, 430.
45. Freskos, J. N.; Fobian, Y. M.; Benson, T. E.; Bienkowski, M. J.; Brown, D. L.; Emmons, T. L.; Heintz, R.; Laborde, A.; McDonald, J. J.; Mischke, B. V. *Bioorg. Med. Chem. Lett.* **2007**, *17*, 73.